Engineering Structures 240 (2021) 112392

Contents lists available at ScienceDirect

Engineering Structures

journal homepage: www.elsevier.com/locate/engstruct

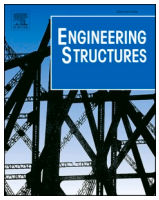

Numerical and analytical study of stainless steel beam-to-column extended end-plate connections

Mohammed M. Eladly *, Benjamin W. Schafer *

Department of Civil and Systems Engineering, Johns Hopkins University, Baltimore, MD, USA

ARTICLE INFO

Keywords:
Stainless steel joints
Beam-to-column joints
End-plate connections
Moment-rotation response
Finite element modeling
Analytical modeling

ABSTRACT

Based on a shell finite element modeling protocol developed and verified by the first author in a previous study, a comprehensive investigation on stainless steel extended end-plate beam-to-column connections was carried out. A total of 180 connection configurations were numerically investigated, to establish a thorough understanding of the influence of a wide range of geometrical parameters on the behavior of this connection type commonly-used in earthquake-resistant steel structures. The initial stiffness; ultimate moment; rotation capacity; dissipative energy; ductility index; and failure patterns were compared and discussed. Furthermore, based on the data acquired from this parametric study, a simple analytical method, for predicting the moment-rotation (M-Φ) characteristics of stainless steel extended end-plate connections, was developed and validated. The results demonstrate that stainless steel extended end-plate connections can be designed to have substantial ductility and rotation capacity, more than satisfactory for beam-to-column joints of structures in seismic zones. In particular, connections with end-plate stiffeners displayed superior performance with enhanced ultimate moment and energy dissipation capacity. The recommended analytical method for M-Φ response of the joints is accurate, with an average error of less than 4% for the ultimate resistance and is robust as evidenced by its prediction of M-Φ response for models that were withheld from its initial calibration. The proposed equations provide, for the first time, a powerful analytical tool that can predict the complete moment-rotation curves of unstiffened and stiffened stainless steel extended end-plate joints, using easy-to-obtain geometric and material properties.

1. Introduction

Due to the excellent mechanical and physical properties; remarkable durability; and pleasant appearance of stainless steel, growing emphasis is being placed on its use in civil and structural engineering [1–5]. The austenitic grades of stainless steel, in particular, have attracted great interest owing to their considerable strain hardening and high ductility which can support their employment in structures subjected to extreme loads (e.g. those in seismic areas) [6–9].

Despite the significant influence of joints on the global performance of frames [10–13], only a small fraction of studies on structural stainless steel have focused on the connections' response. Most of these investigations (i.e. investigations on stainless steel connections) were conducted into simple or lap joints [14–35], while the studies on beam-to-column connections are scarce [36–42]. Such studies on beam-to-column connections are essential for the evaluation of the current design rules for stainless steel joints (in Eurocode 3 [43,44], as well as other international structural design standards) which copy those of carbon steel joints, neglecting the ductile nature and strain hardening characteristics of stainless steel alloys.

Among the different types of beam-to-column connections utilized in the structural steel industry, extended end-plate joints have gained wide popularity, because of their reasonable cost, and the ease of their manufacture and installation. Studies on carbon steel extended end-plate connections [45–46] demonstrated that this type of connection can obtain nearly the same initial rigidity and ultimate moment capacity of fully-welded joints, but with higher ductility and greater dissipative energy, which results in a superior performance from a structural point of view. Nevertheless, to date, there is no comprehensive study exploring the behavior of this promising connection type when made from stainless steel; the few published parametric investigations on stainless steel extended end-plate joints [38,41,42] have not considered the effects of influential parameters, such as bolt diameter; beam depth; and the presence of end-plate rib stiffeners.

In this paper, the first exhaustive numerical parametric analysis of stainless steel extended end-plate beam-to-column connections (carried

* Corresponding authors.
E-mail addresses: eladly@ymail.com, eladly@jhu.edu (M.M. Eladly), schafer@jhu.edu (B.W. Schafer).

https://doi.org/10.1016/j.engstruct.2021.112392
Received 18 November 2020; Received in revised form 12 March 2021; Accepted 11 April 2021
Available online 4 May 2021

out using the simplified numerical model constructed and verified by Eladly [47]) is reported. The effects of various key parameters on ultimate resistance; initial rigidity; plastic moment resistance; energy dissipation capacity; ductility; and failure modes were investigated in the study. After that, the resulting finite element (FE) data were exploited to formulate and evaluate an analytical method able to predict the moment-rotation response of stainless steel end-plate joints. Finally, the accuracy of that proposed method was further examined by comparison with numerical results for additional connection configurations other than those considered in the parametric study.

2. Finite element modeling

The finite element study presented in the current paper was performed (using the general-purpose FE simulation software ABAQUS [48]) based on the simplified numerical model developed by the first author in an earlier investigation [47]. The model's ability to simulate the response of stainless steel beam-to-column bolted connections has already been validated using experimental results [47] and hence, is not repeated herein. However, for completeness and convenience, a brief description of the model is presented in the current section.

Four-node stress/displacement shell elements with reduced integration (S4R) were adopted for all connection components. To account for the nonlinear effects of large displacements that beam-to-column bolted connections can experience, geometric nonlinearity was considered. CARTESIAN elements [48] were chosen to represent stainless steel bolts, with "Elasticity and Plasticity" behaviors defined in all the three directions (i.e. the bolt axial force direction in addition to the two bolt shear force directions). To avoid the occurrence of the excessive local plastic deformations that may take place at any two nodes connected by a CARTESIAN element and to accurately capture the effects of bolts' heads and nuts, "Rigid Body" constraints [48] were utilized. In terms of the interactions between the non-welded parts of connections (e.g. between column flange and end-plate), the surface-to-surface contact was employed. "Hard" contact relationship was used for the normal interaction, whilst for the tangential interaction, "Coulomb friction" formulation with a friction coefficient of 0.3 was utilized. For representing the response of stainless steel material, the two-stage Ramberg-Osgood material model [49], adopted by Eurocode 3-Part 1.4 [43], was used to calculate the nominal stresses and strains, which were then converted into the format of true stresses and log plastic strains before inputting into ABAQUS.

As explained in detail in [47], validating the model against the results of full-scale tests on stainless steel beam-to-column bolted connections showed the great accuracy of the model in predicting the moment-rotation responses and failure patterns of different connection types. However, it is noteworthy that producing the falling parts of the moment-rotation curves was beyond the capability of the model, since the FE analysis stopped due to reaching the limiting values of plastic motion in the axial and/or shear force direction of CARTESIAN elements representing bolts [47] (which was in line with the experimentally-observed failure that was triggered by bolts' fracture in tension and/or shear [37]). Nevertheless, this inability of the model to provide the falling portions of responses did not negatively influence its effectiveness in predicting the ultimate moment capacities $M_{j,\max}$, the moment-rotation responses until failure, and the failure modes of joints [47].

3. Parametric study

Using the FE model described in the previous section, an extensive numerical parametric investigation on austenitic stainless steel extended end-plate beam-to-column connections was undertaken. The results derived from this investigation are thoroughly analyzed in Section 4 to gain a comprehensive understanding of the behavior of extended end-plate connections made of stainless steel, and then employed in Section 5 to develop a simple analytical technique for predicting the M-Φ response of these connections.

The end-plate extended-on-both-sides connection configuration was chosen to be investigated in the current study, as this type of connection is recommended to be used in earthquake-resistant carbon steel structures because of its excellent structural performance and great energy dissipation capacity when compared to other connection types (e.g. welded or flush end-plate connections) [50–52]. A total of 180 connections were researched in the study, in order to cover the geometric parameters that have been found to be influential in the connection rotational behavior in previous investigations into carbon steel extended end-plate joints [52–57]. These parameters include end-plate thickness (t_p); column flange thickness (t_{fc}); horizontal bolts gauge (g); the vertical distances between the bolt rows in tension (the two top bolt rows) and the centerline of the beam compression flange (Z_1 and Z_2); beam depth (d); bolt diameter (D); and end-plate rib stiffeners' thickness (t_{rs}). In addition to the above geometric properties, two austenitic stainless steel grades were considered in the parametric analysis (i.e. EN 1.4301 and EN 1.4307 whose material parameters can be found in [37,47;58], respectively). A Schematic outline of the extended end-plate joints examined in the study is displayed in Fig. 1(a), whilst a detailed description is presented in Fig. 1(b), with fixed values for the dimensions kept unchanged in all studied cases and symbols for the variable dimensions.

Table 1 reports a summary of the investigated parameters, including the key geometric dimensions in addition to stainless steel grade. t_p; t_{fc}; g; Z_1; Z_2; d; D; and t_{rs} were varied as shown in the table, while the remaining dimensions of the I-section columns and beams were identical to those tested by Elflah et al. [37]. The column in all connections had an outer depth of 240 mm; a flange width of 120 mm; and a web thickness of 10 mm, whereas the flange thickness was varied, as illustrated in Table 1. With regard to the beam, the flange width; flange thickness; and web thickness were, respectively, 120; 12; and 10 mm in all considered cases, whilst the beam depth was one of the examined parameters (Table 1). The values of the variable dimensions and the used stainless steel grades for the 180 investigated connections are detailed in Eladly's dataset [59]. These values have been varied so that the investigated cases cover both the conditions satisfying and violating the provisions of Eurocode 3 [43,44] as well as those recommended by Shi et al. [52] for end-plate connections. Given the fact that the current study focuses on the connections' response, the studied joints have been so designed that the failure is confined in the connection zone. Thus, all connections were partial-strength connections, and as a result of their geometry they were also semi-rigid.

As illustrated in Fig. 1(a), the lower end of the column was fixed, while the upper end had restrained horizontal displacements in the plane of loading. A vertical monotonic load was imposed on the beam's end at 1.47 m from the column face (Fig. 1(a)), with preventing the out-of-plane deformations. Bolt preloading was outside the scope of the study and hence no pretension forces were applied to the grade A80 stainless steel bolts utilized for connection (the material characteristics of the employed bolts are reported in [37]). Throughout the parametric analysis, the columns were stiffened with 12 mm thick stiffeners (Fig. 1), while the presence and thickness of end-plate triangle rib stiffeners was one of the parameters researched, as explained in Table 1.

Connection moment (M) was calculated by multiplying the force applied on the beam's end by the distance from the imposed force to the column face (1.47 m), while connection rotation (Φ) was determined from the relative rotation of the centerlines of the flanges of beam at connection region [52].

The results of the investigation are presented and discussed in the following section in terms of initial stiffness; ultimate moment capacity; rotation corresponding to ultimate moment capacity; moment at 30 mrad; plastic moment resistance; energy dissipation capacity; and ductility index. The descriptions and symbols of these seven indicators are provided in Table 2.

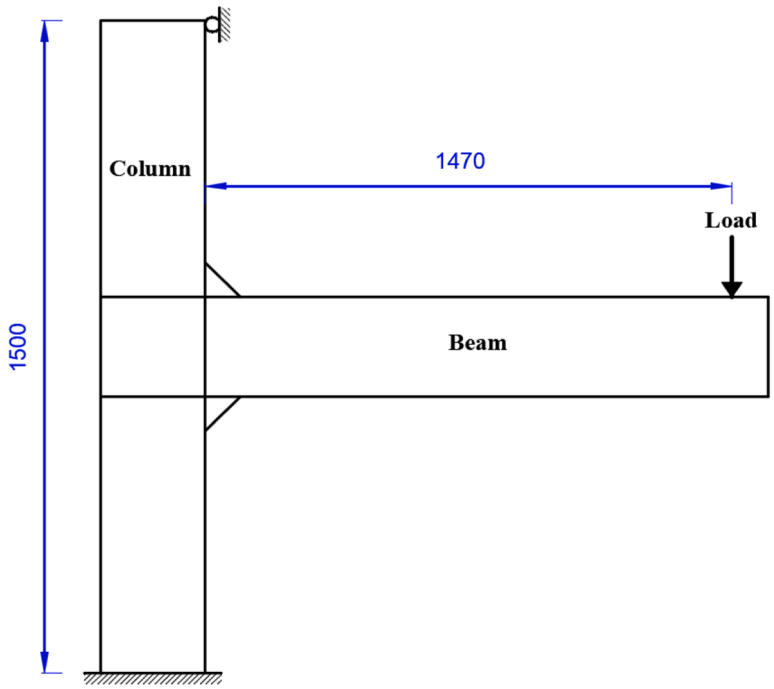

(a) Schematic outline

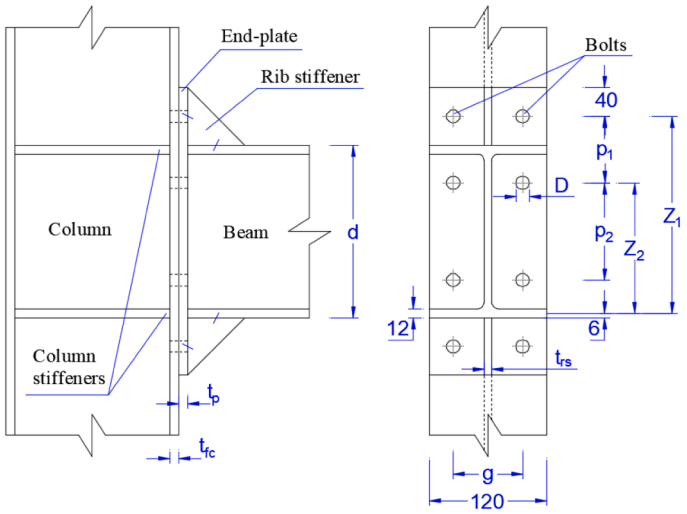

(b) Detailed dimensions (the dimensions corresponding to the symbols for the 180 studied connections can be found in Eladly's dataset [59])

Fig. 1. Description of extended end-plate connections investigated in the parametric study (all dimensions are in mm).

Table 1
Values of geometric and material parameters investigated in the parametric study (see Fig. 1(b) for the meanings of symbols).

t_p mm)	t_{fc} (mm)	g (mm)	Z_1 (mm)	Z_2 (mm)	d (mm)	D (mm)	End-plate rib stiffeners	Stainless steel grade
8	12	50	274	162	240	12	Unstiffened	EN 1.4301
10	14	70	294	182	300	16	Stiffened, t_{rs} = 6 mm	EN 1.4307
12	–	–	334	242	–	–	Stiffened, t_{rs} = 10 mm	–

4. Results and discussion

Table 3 reports the key numerical results for stainless steel extended end-plate connections subjected to bending moment. In each case, only one parameter was changed, while the others were set to fixed values. For ease of identification, the changed parameter for each model presented in the table has been underlined and highlighted in bold.

From the table, it is clear that stainless steel beam-to-column joints have significant ductility, as demonstrated by the ductility index (ψ_j) which ranged from 3.74 to 6.78 for the cases listed in the table and from 3.04 to 6.90 for all investigated cases. In terms of ultimate rotation ($\Phi_{j,u}$), all joints researched in the study satisfied the rotation capacity of 30 mrad recommended by [60–62,65] for connections in steel moment-resisting frames in seismic zones.

Table 2
Symbols and descriptions of the indicators used in the parametric study.

Symbol	Description
$S_{j,ini}$	**Initial stiffness**: the slope of the moment-rotation curve at the origin.
$M_{j,max}$	**Ultimate moment capacity**
$\Phi_{j,u}$	**Rotation corresponding to ultimate moment capacity**
$M_{j,30}$	**Moment at 30 mrad** which is commonly deemed an adequate rotation capacity for beam-to-column connections [60–62].
$M_{j,R}$	**Plastic moment resistance** which can be calculated using the method described in [63], wherein the plastic resistance is determined from the intersection between the initial stiffness and the hardening stiffness lines in the moment-rotation curve. This method has been widely adopted in previous researches on the response of connections [37,38,61,62].
E_d	**Energy dissipation capacity** which can be computed from the area under force–displacement curve.
ψ_j	**Ductility index**: this parameter quantifies the length of the yield plateau of the moment-rotation response for a connection as an indicator of its ductility characteristics. Ductility index can be determined by dividing the rotation value at ultimate moment by the rotation corresponding to plastic moment resistance [64].

With increasing the imposed loading, the finite element models showed considerable inelastic deformations in end-plates (i.e. a typical failure mode of t-stub joints) as well as in column flanges until the connections' failure occurred (Fig. 2). This failure, for all studied joints, was prompted by bolts failure in tension, due to the limited ductility of bolts (as evidenced by their relatively low plastic strain at fracture ($\varepsilon_f = 0.12$)), when compared to other connection components with ε_f ranging from 0.54 to 0.66 (Table 1 in Eladly's FE study [47]).

To interpret the physical response of joints, a brief explanation of the components of joint rotation should be firstly provided. The joint rotation (Φ) incorporates two parts: the shearing rotation (Φ_s) induced by the panel zone deformation, and the gap rotation (Φ_{ep}) resulting from the relative deformation between the end-plate and the column flange including the bending deformation of the end-plate in addition to the extension of the bolts (Fig. 2). Φ_s; Φ_{ep}; and Φ are defined in Eq. (1).

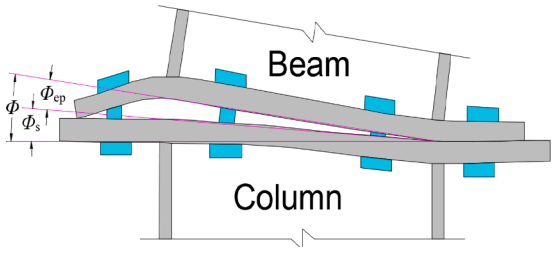

Fig. 2. Definition of connection rotation.

Table 3
Key FE results extracted from the M-Φ curves (see Fig. 1(b) and Table 2 for the meanings of symbols).

Model ID	t_p (mm)	t_{fc}	g	Z_1	Z_2	d	D	End-plate rib stiffeners	Stainless steel grade	$S_{j,ini}$ (kN.m/rad)	$M_{j,max}$ (kN.m)	$\Phi_{j,u}$ (mrad)	$M_{j,30}$ (kN.m)	$M_{j,R}$ (kN.m)	E_d (kN.mm)	ψ_j
Model-073	**10**	12	70	294	162	240	16	Unstiffened	EN 1.4301	5661	79.60	90.45	54.77	47.25	5263	4.79
Model-075	**8**	12	70	294	162	240	16	Unstiffened	EN 1.4301	4705	75.75	104.75	42.25	37.62	5344	4.99
Model-077	**12**	12	70	294	162	240	16	Unstiffened	EN 1.4301	6510	83.04	74.50	63.99	55.98	4683	4.09
Model-111	8	**12**	70	334	242	300	16	Unstiffened	EN 1.4301	11,237	108.85	67.82	76.82	56.43	5225	6.41
Model-112	8	**14**	70	334	242	300	16	Unstiffened	EN 1.4301	11,556	110.11	66.81	77.19	57.04	5160	6.22
Model-005	12	12	**70**	274	182	240	16	Unstiffened	EN 1.4301	9134	91.02	53.19	75.90	61.02	3661	4.65
Model-041	12	12	**50**	274	182	240	16	Unstiffened	EN 1.4301	9904	93.05	50.86	79.13	63.88	3605	4.07
Model-028	8	14	**70**	274	182	240	16	Stiffened, t_{rs} = 10 mm	EN 1.4301	11,628	109.40	69.58	81.49	66.24	5646	5.45
Model-064	8	14	**50**	274	182	240	16	Stiffened, t_{rs} = 10 mm	EN 1.4301	13,945	118.33	63.51	94.61	75.17	5781	5.89
Model-001	10	12	70	**274**	182	240	16	Unstiffened	EN 1.4301	8181	90.02	70.52	68.05	57.20	4749	4.74
Model-145	10	12	70	**294**	182	240	16	Unstiffened	EN 1.4301	6781	80.77	75.21	58.91	50.31	4477	4.19
Model-014	10	14	70	**274**	182	240	16	Stiffened, t_{rs} = 6 mm	EN 1.4301	12,535	113.28	69.05	88.17	75.44	5995	4.74
Model-152	10	14	70	**294**	182	240	16	Stiffened, t_{rs} = 6 mm	EN 1.4301	12,481	111.55	72.45	86.51	75.26	6234	4.80
Model-087	8	12	70	294	**162**	240	16	Stiffened, t_{rs} = 6 mm	EN 1.4301	9711	107.31	108.21	70.54	61.19	8631	6.78
Model-153	8	12	70	294	**182**	240	16	Stiffened, t_{rs} = 6 mm	EN 1.4301	10,640	106.47	90.43	73.84	61.42	7184	6.16
Model-002	10	14	70	274	182	**240**	16	Unstiffened	EN 1.4301	8456	90.70	68.51	68.83	57.28	4634	4.80
Model-110	10	14	70	334	242	**300**	16	Unstiffened	EN 1.4301	14,200	112.68	50.48	93.89	72.28	4253	4.89
Model-169	10	12	70	274	182	240	**16**	Stiffened, t_{rs} = 6 mm	EN 1.4307	11,849	113.15	65.60	90.51	77.57	5732	4.41
Model-175	10	12	70	274	182	240	**12**	Stiffened, t_{rs} = 6 mm	EN 1.4307	9741	76.73	43.89	68.67	54.35	2588	3.74
Model-040	8	14	50	274	182	240	16	**Unstiffened**	EN 1.4301	8044	88.19	73.80	63.24	52.53	4737	5.18
Model-052	8	14	50	274	182	240	16	**Stiffened, t_{rs} = 6 mm**	EN 1.4301	13,176	109.50	67.21	85.38	72.02	5620	4.85
Model-064	8	14	50	274	182	240	16	**Stiffened, t_{rs} = 10 mm**	EN 1.4301	13,945	118.33	63.51	94.61	75.17	5781	5.89

$$\Phi_s = \Delta/d_f \quad (1a)$$

$$\Phi_{ep} = \delta/d_f \quad (1b)$$

$$\Phi = \Phi_s + \Phi_{ep} \quad (1c)$$

where Δ is the difference between the displacements of column flange points at the centerlines of the beam flanges; δ is the gap width between the end-plate and the column flange at the beam tension flange centerline; and d_f is the distance between the centerlines of the beam flanges.

Figs. 3 and 4 illustrate the effect of end-plate thickness on the failure modes and moment-rotation characteristics of connections. As expected, an increase in end-plate thickness (t_p) resulted in an enhancement of its bending stiffness and in turn a decrease in the gap rotation (Φ_{ep}) which constitutes the greatest part of the total rotation (Fig. 2). Consequently, an obvious rise in the resistance of the equivalent T-stub [66] took place, and the tension bolts' fracture occurred at higher applied loads (i.e. the ultimate moment capacity of connections increased). This increase in strength was accompanied by corresponding increase in stiffness; plastic moment resistance; and moment at 30 mrad, with noticeable decrease in rotation capacity; dissipative energy; and ductility (Table 3). It is noteworthy that using end-plate stiffeners reduced this impact of end-plate thickness, as shown in Fig. 4.

From Fig. 5, it can be observed that column flange thickness does not have a notable effect on the connections' behavior for the range of parameters investigated. This is not surprising since the contribution of shearing rotation (Φ_s), caused by the panel zone deformation, to the connection rotation (Φ) is relatively small. Hence, using stiffer column flange, which affects Φ_s only, has a slight impact on the overall joint rotation capacity and therefore increasing flange thickness led to marginal enhancements of strength and stiffness.

As for bolts gauge (g), it had a marked influence on the response of joints stiffened with end-plate stiffeners (Fig. 6(b)) and a less-pronounced effect in the case of unstiffened connections (Fig. 6(a)). In both cases, increasing the horizontal bolts gauge caused a decrease in the joints' rigidity and ultimate moment, together with a rise in rotation capacity and ductility, as detailed in Table 3. Similar conclusions were reported by Elflah et al. [38]. The above observations can be interpreted in terms of failure modes. As seen in Fig. 7, bending of end-plate in the out-of-plane direction is obvious in the case of stiffened joints, while it is not noticeable for unstiffened connections. This bending causes an evident gap between end-plate and column flange which contributes to (Φ_{ep}) and in turn to the overall connection rotation. Using smaller bolts gauge greatly helps in decreasing this gap that results from the out-of-plane bending of end-plate and consequently diminishes the total joint rotation. From the above, it is not surprising that the strength and stiffness of connections with end-plate stiffeners were enhanced due to decreasing bolts gauge.

Fig. 8 depicts the moment-rotation curves of connections with different Z_1 (where Z_1 is the vertical distance between the outer bolt row in tension and the centerline of the beam compression flange, as displayed in Fig. 1(b)). In the case of unstiffened end-plate connections (Fig. 8(a)), there were obvious rises in the maximum moment and initial stiffness of connections with decreasing Z_1. The reason for this is that when Z_1 becomes smaller, the outer tension bolts become closer to the tension beam flange, which helps in decreasing the deformation of t-stub consisting of the tension flange of beam and the end-plate between the two bolt rows in tension. Reducing this deformation, which is the main contributor to Φ_{ep}, improves the rotation capacity of connections and in turn enhances the stiffness and ultimate moment. On the other hand, the response of connections with stiffened end-plates was independent of the magnitude of Z_1, as illustrated in Fig. 8(b). These very similar behaviors of stiffened joints with different Z_1 can be attributed to the fact that increasing Z_1 (with maintaining the same beam's depth) is naturally accompanied by an increase in the extended part of the end-plate and consequently in the volumes of end-plate stiffeners. These enhancements of stiffeners' volumes produce improvements in the stiffness and ultimate capacity of joints, which offset the reduction in these two parameters resulting from increasing Z_1, leading finally to a trivial difference between the M-Φ responses of stiffened connections with varied Z_1.

Contrary to Z_1, Z_2 (the distance of the inner bolt row in tension from the beam compression flange's centerline) had an inverse relation with ultimate rotation and dissipative energy of joints, as can be observed in Fig. 9 and Table 3. This is due to the fact that decreasing Z_2 makes the the inner bolt row in tension more distant from the tension beam flange. Thus, the t-stub deformation increases, leading to a rise in the connection's maximum rotation. It can also be noted that despite the clear difference in stiffness associated with changing Z_2, the ultimate moment of connections with varied Z_2 remained unaffected, which is attributable to the rise in the maximum rotations of the less-stiffer joints, which compensated for the reduced rigidity.

Figs. 10 and 11, respectively, display the M-Φ curves of connections with different beam depths and bolts diameters. From the figures, it can be seen that both parameters have a direct correlation with the strength and stiffness of connections. Assigning a beam depth of 300 mm instead

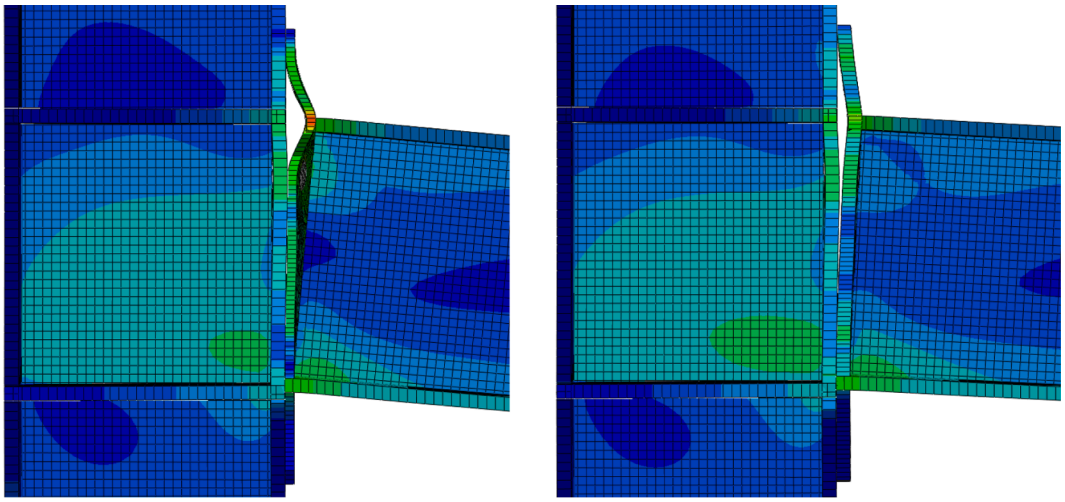

(a) t_p = 8 mm (b) t_p = 12 mm

Fig. 3. Comparison of deformations and stress distribution in two extended end-plate connections with different end-plate thicknesses (both subjected to a bending moment of 85 *kN.m*).

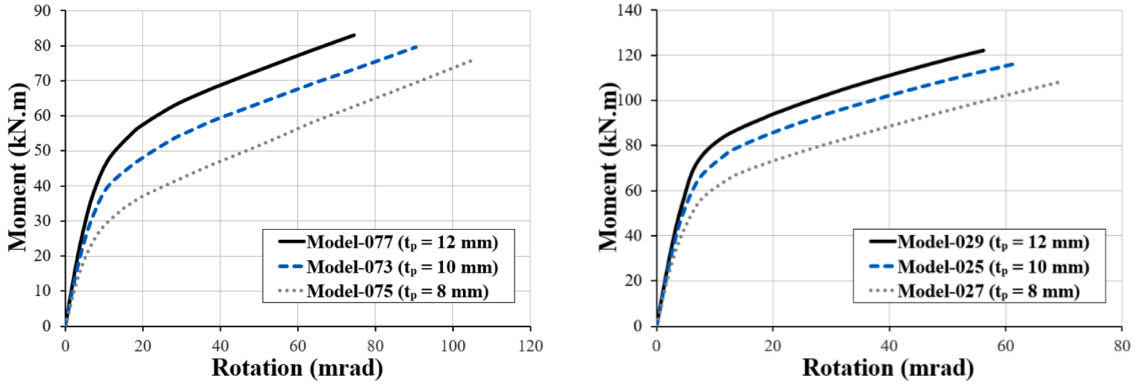

(a) Without end-plate stiffeners (b) With end-plate stiffeners

Fig. 4. Moment-rotation curves for connections with end-plates of different thicknesses.

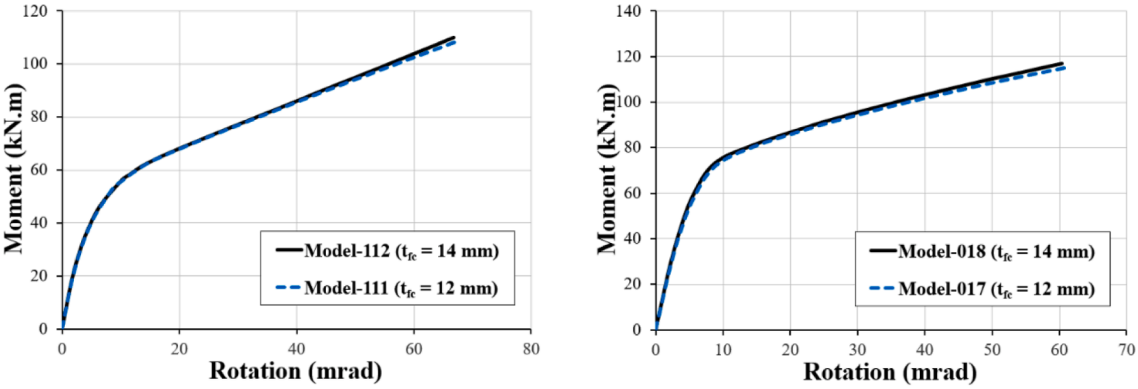

(a) Without end-plate stiffeners (b) With end-plate stiffeners

Fig. 5. Effect of column flange thickness on connections' moment-rotation response.

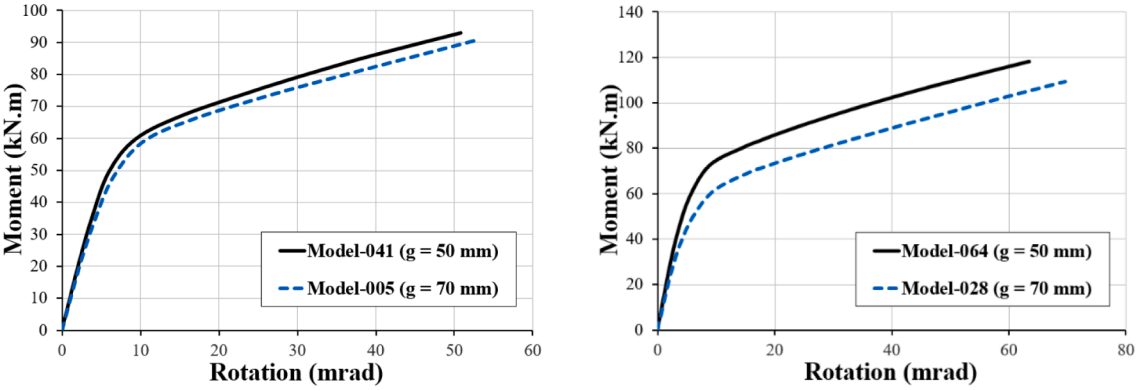

(a) Without end-plate stiffeners (b) With end-plate stiffeners

Fig. 6. Effect of bolts gauge on joints' moment-rotation behavior.

of 240 mm raised the moment capacity by 25%, whilst increasing bolts diameters from 12 mm to 16 mm resulted in an ultimate moment improvement of nearly 50% (Table 3). The only remarkable difference between the two parameters was in their influence on the rotation capacity. The effect of beam depth followed the trends observed in other parameters (discussed above) with the ultimate rotation improving with the stiffness decrease (Fig. 10). Increasing beam depth caused a corresponding increase in the bending stiffness of both beam and end-plate, and consequently decreased the gap rotation (Φ_{ep}) which results mainly from end-plate bending. This led to a response with higher stiffness and strength.

On the other hand, using bolts with larger diameters led to a stiffer response together with a greater rotation capacity which both produced a dramatic enhancement of the ultimate moment, as shown in Fig. 11. This is not unexpected, since the failure of joints was triggered by bolts fracture (as previously mentioned) and accordingly increasing the

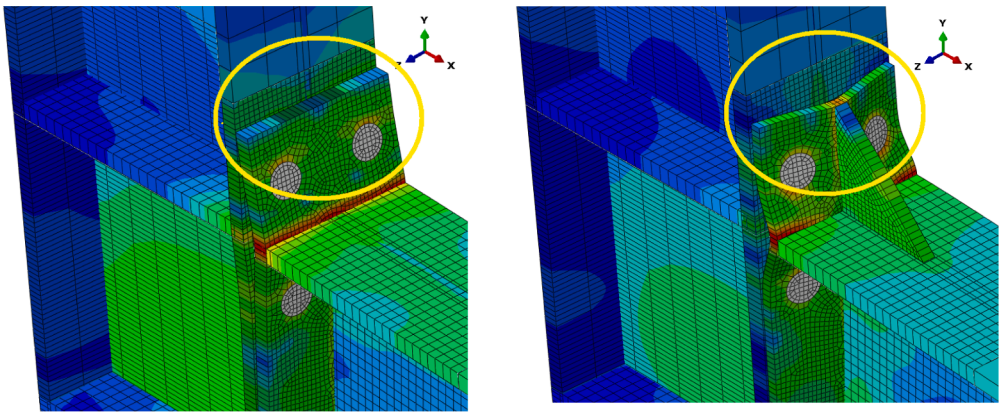

(a) Without end-plate stiffeners (b) With end-plate stiffeners

Fig. 7. Deformed shapes of joints with and without end-plate stiffeners.

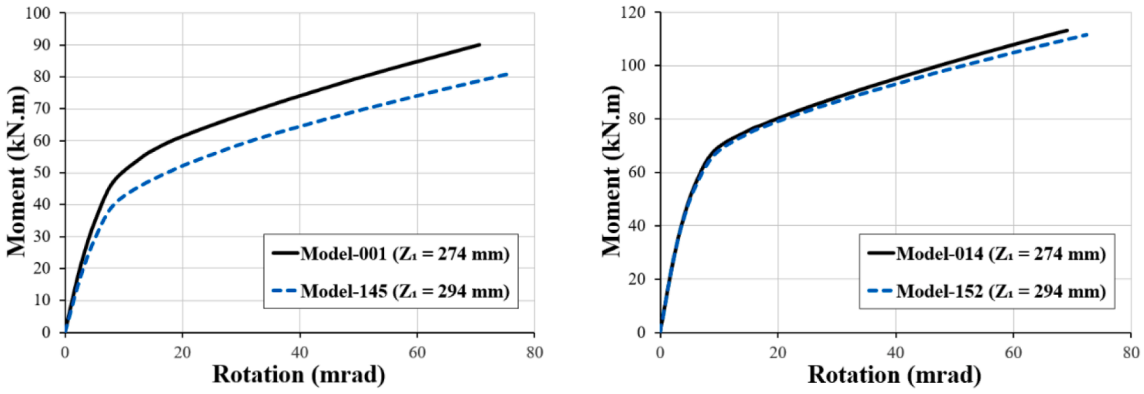

(a) Without end-plate stiffeners (b) With end-plate stiffeners

Fig. 8. Influence of Z_1 on the moment-rotation characteristics of connections.

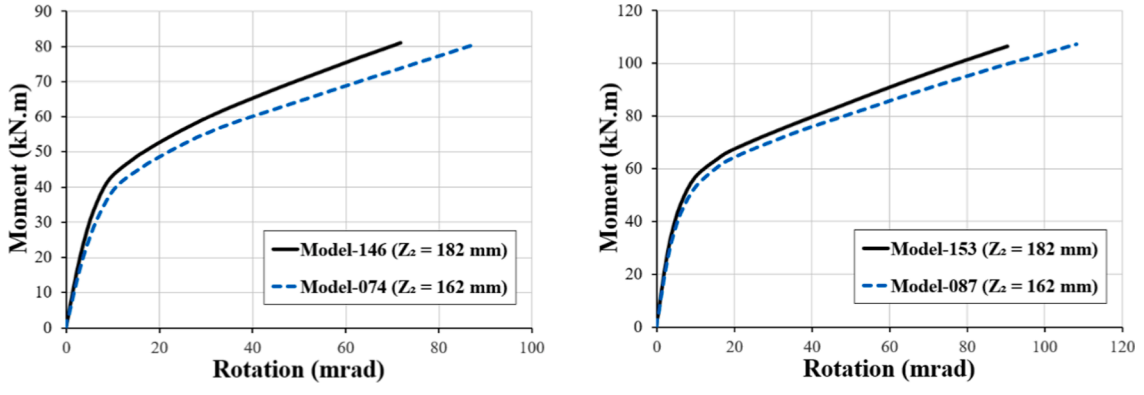

(a) Without end-plate stiffeners (b) With end-plate stiffeners

Fig. 9. Influence of Z_2 on the moment-rotation characteristics of connections.

diameters of bolts (the weakest components of the connection) enhances simultaneously stiffness and rotation capacity. On the contrary, improving the stiffness of other connection parts (e.g. increasing end-plate thickness) puts greater stresses on bolts at relatively lower connection rotations, causing eventually a reduction in the maximum rotation.

Fig. 12 presents the deformation and stress distribution in joints with and without end-plate stiffeners. From the figure, it could be concluded that end-plate stiffeners can be considered as the first line of defense in extended end-plate joints; their use causes the plastic strains to be concentrated on the stiffeners themselves and consequently decreases the strains and stresses on other connection components (e.g. end-plate and column flange). Employing these rib stiffeners results in a dramatic enhancement of end-plate stiffness and thus a decrease in the associated rotation (i.e. Φ_{ep}), which delays the occurrence of bolts' fracture in tension and hence induces an evident rise in the strength and energy dissipation capacity of connections (Fig. 13 and Table 3). The benefits of these stiffening elements strongly support their utilization in end-plate

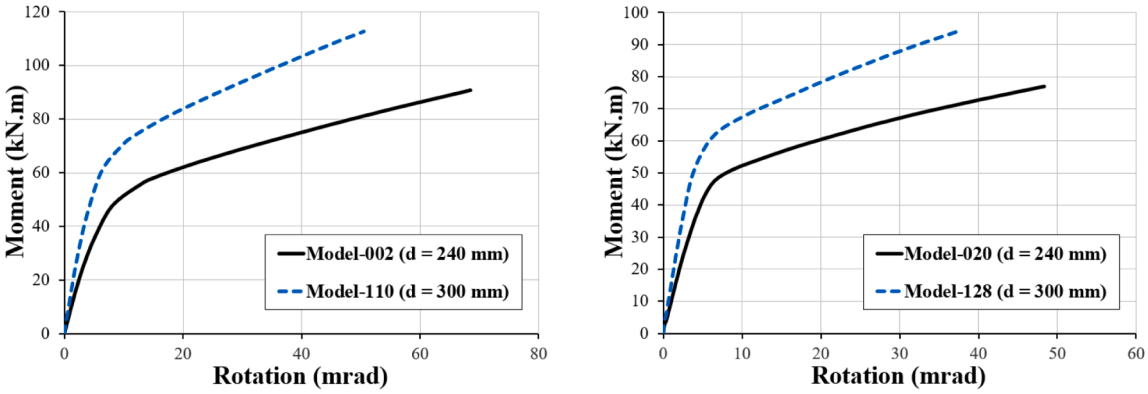

(a) Without end-plate stiffeners (b) With end-plate stiffeners

Fig. 10. Moment-rotation curves for connections with different beam depths.

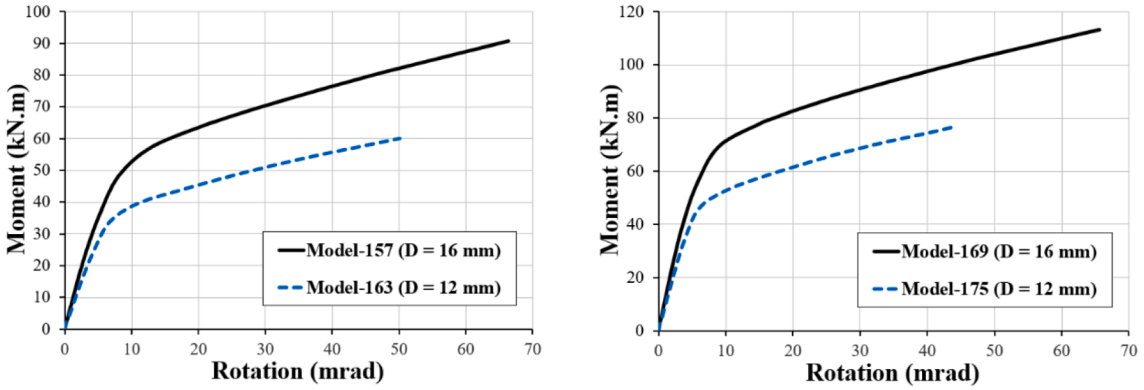

(a) Without end-plate stiffeners (b) With end-plate stiffeners

Fig. 11. Effect of bolts diameter on connections' moment-rotation behavior.

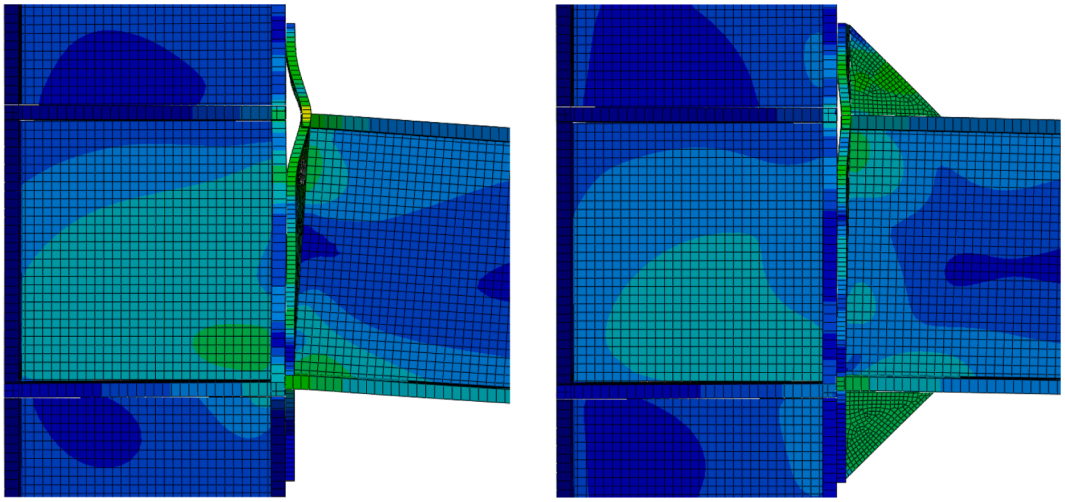

(a) Unstiffened (b) Stiffened

Fig. 12. Effect of end-plate stiffeners on deformation and stress distribution in extended end-plate joints (both connections under a bending moment of 85 *kN.m*).

joints in stainless steel structures prone to seismic actions. This conclusion agrees with the results of corresponding studies on carbon steel extended end-plate joints [45,52].

5. Analytical model of stainless steel extended end-plate connections

Based on the FE data for the 180 cases investigated in the parametric study, an analytical method for determining the moment-rotation

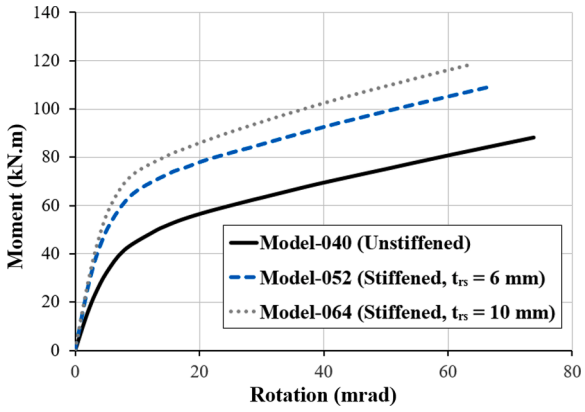

Fig. 13. Impact of end-plate stiffeners on the moment-rotation response of joints.

characteristics of stainless steel extended end-plate connections was proposed. To formulate this method, the four-parameter model suggested by Richard and Abbott [67], for moment-rotation relationships, was employed. Richard and Abbott model was chosen, due to its simplicity as it requires a relatively small number of parameters (only four). Moreover, it considers the strain-hardening properties of materials and hence can accurately predict the behavior of ductile materials having great strain hardening such as stainless steel. It is noteworthy that Richard-Abbott model has been used in a previous analytical investigation into stainless steel top-seat angle connections, producing satisfying results [36].

A preliminary analytical study was performed by the first author [69] on unstiffened extended end-plate connections adopting the same approach used herein. However, this previous study has some shortcomings. It was performed on unstiffened extended end-plate connections only without considering the effect of end-plate stiffeners; the number of FE models used in the calibration of the analytical model was relatively small; the analytically-predicted curves can progress unceasingly with no specific maximum moment/rotation; and the applications and limitations of the suggested analytical method were not discussed. The analytical study reported in the current paper tries to tackle the above shortcomings.

5.1. Description of the four-parameter model

Richard and Abbott [67] developed a nonlinear mathematical formula for the relationship between the moment (M) and the rotation (Φ). This formula is applicable to different types of joints with various forms of responses (e.g. strain hardening; strain softening; and strain stiffening responses). Four parameters (i.e. K_i, K_p, M_o, N) are incorporated by Richard-Abbott formula, as given by Eq. (2).

$$M = \frac{(K_i - K_p)\phi}{\left(1 + \left|\frac{(K_i - K_p)\phi}{M_O}\right|^N\right)^{1/N}} + K_p\phi \quad (2)$$

where M is the connection moment; Φ is the connection rotation; K_i is the initial (or elastic) stiffness; K_p is the strain-hardening (or plastic) stiffness; M_o is the reference moment; and N is the curve shape factor. The definition of each of these parameters on a typical moment-rotation curve can be seen in Fig. 14.

Richard-Abbott general M-Φ curve presented in Fig. 14 meets the boundary requirements of moment-rotation curves of monotonically-loaded extended end-plate connections. These requirements include:

(i) The curve starts at the origin (i.e. moment at *zero rad* is equal to *zero*).

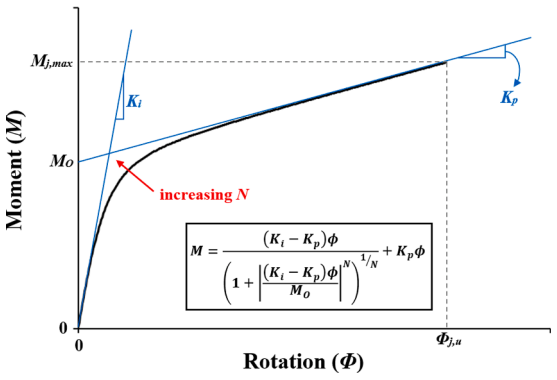

Fig. 14. Richard and Abbott [67] equation for defining moment-rotation relationships.

(ii) The connection elastic stiffness (K_i) equals the slope of the moment-rotation curve at the origin.
(iii) For any given rotation, the connection tangent stiffness can be calculated from the slope of the moment-rotation curve at that rotational angle.
(iv) With increasing the rotation, the curve slope becomes closer to the strain-hardening stiffness (K_p).

5.2. Development and validation of functions for the four parameters

Moment-rotation curves are the ultimate outcome of very complicated interactions among the connected members' components (e.g. column flange, beam flange) and the connecting parts (e.g. end-plate, bolts). Hence, it is necessary to take into account the effect of each of these influential connection components while developing an analytical method for predicting the M-Φ response of joints.

The analytical model suggested in the current section for stainless steel extended end-plate connections incorporates the impact of the significant geometric and material properties that have been examined in the parametric study presented in Sections 3 and 4. The considered properties include end-plate thickness (t_p); column flange thickness (t_{fc}); horizontal bolts gauge (g); the vertical distances between the bolt rows in tension and the centerline of the beam compression flange (Z_1 and Z_2); beam depth (d); bolt diameter (D); end-plate rib stiffeners' thickness (t_{rs}); and stainless steel grade. These geometric and material properties are easy-to-obtain, which greatly enhances the usability of the suggested analytical technique.

According to Richard and Abbott expression [67] shown in Eq. (2), four parameters are needed to determine the M-Φ characteristics of joints (i.e. K_i, K_p, M_o, and N). Thus, a function for each of these four parameters should be formulated, in order to analytically predict the entire moment-rotation behavior of connections. However, as the presence of end-plate stiffeners significantly changes the failure mode and the response of joints (as discussed earlier in Section 4), two functions were developed for each of the four parameters: one in the case of connections without end-plate stiffeners and the other for the stiffened connections.

Depending on nonlinear regression analysis of finite element results and after considering different types of functions (e.g. linear, power, exponential), expressions for K_i; K_p; M_o; and N were determined in terms of the above-mentioned geometric and material properties, as listed in Table 4. The power form of equation was chosen for the expressions, due to its straightforwardness during statistical analysis and, more importantly, because it facilitates the observation of the impact of single geometrical/material properties on the four connection parameters and consequently on the complete moment-rotation response. For instance, the positive values of the exponents of end-plate thickness (t_p) in the developed functions indicate a direct correlation between this

Table 4
Four parameters' expressions for unstiffened and stiffened stainless steel extended end-plate joints.

	Parameter	Unit	Function	
Unstiffened	K_i	*kN.m/rad*	$1.24 \times 10^{-5} \times t_p^{0.809} \times t_{fc}^{0.305} \times g^{-0.238} \times (d\text{-}Z_2)^{-0.129} \times (Z_1\text{-}d)^{-0.152} \times d^{2.664} \times D^{0.955} \times \sigma_{0.2}^{0.058} \times E^{0.173}$	(3)
	K_p	*kN.m/rad*	$1.223 \times 10^{-5} \times t_p^{0.39} \times t_{fc}^{0.225} \times g^{-0.25} \times (d\text{-}Z_2)^{-0.1} \times (Z_1\text{-}d)^{-0.125} \times d^{2.852} \times D^{0.6432} \times \sigma_{0.2}^{0.0742} \times \sigma_u^{0.0208}$	(4)
	M_o	*kN.m*	$2.966 \times 10^{-4} \times t_p^{1.0238} \times g^{-0.11} \times (d\text{-}Z_2)^{-0.1274} \times (Z_1\text{-}d)^{-0.18} \times d^{1.04506} \times D^{1.171} \times \sigma_{0.2}^{0.42}$	(5)
	N	*dimensionless*	$2.6 \times 10^{-3} \times t_p^{0.904} \times t_{fc}^{0.377} \times g^{-0.214} \times (d\text{-}Z_2)^{-0.24} \times (Z_1\text{-}d)^{-0.209} \times d^{0.492} \times D^{-0.592} \times \sigma_{0.2}^{0.948}$	(6)
Stiffened	K_i	*kN.m/rad*	$1.064 \times 10^{-6} \times t_p^{0.512} \times t_{fc}^{0.149} \times g^{-0.2} \times (d\text{-}Z_2)^{-0.188} \times (Z_1\text{-}d)^{-0.02} \times d^{1.893} \times D^{0.7741} \times \sigma_{0.2}^{0.221} \times E^{0.7687} \times t_{rs}^{0.11}$	(7)
	K_p	*kN.m/rad*	$1.01 \times 10^{-4} \times t_p^{0.85} \times t_{fc}^{0.267} \times g^{-0.31} \times (d\text{-}Z_2)^{-0.191} \times (Z_1\text{-}d)^{-0.159} \times d^{2.4256} \times D^{0.319} \times \sigma_{0.2}^{0.1} \times \sigma_u^{0.033} \times t_{rs}^{0.375}$	(8)
	M_o	*kN.m*	$2.83 \times 10^{-3} \times t_p^{0.553} \times g^{-0.04} \times d^{0.714} \times D^{1.31} \times \sigma_{0.2}^{0.261} \times t_{rs}^{0.03}$	(9)
	N	*dimensionless*	$8.5 \times 10^{-4} \times t_p^{0.8} \times t_{fc}^{0.122} \times g^{-0.302} \times (d\text{-}Z_2)^{-0.156} \times (Z_1\text{-}d)^{-0.045} \times d^{0.52} \times D^{-0.565} \times \sigma_{0.2}^{1.0535} \times t_{rs}^{0.33}$	(10)

[Note]: The geometric and material characteristics are expressed in mm and N/mm^2, respectively.

characteristic and the stiffness and strength of connections; this agrees with the observations made in Section 4 concerning the influence of end-plate thickness. Another example is the negative exponents of bolts gauge (g) which are consistent with the conclusion reached in the previous section that bolts gauge is in inverse proportion to the rigidity and ultimate capacity of joints. Additionally, the adopted equation form allows easy comparison between the extent of the effects of different geometrical parameters. For example, the exponents of end-plate thickness (t_p) in the derived equations are remarkably larger than their counterparts for column flange thickness (t_{fc}), which is in line with the discussion in Section 4 which shows that the impact of t_p on the M-Φ behavior is more pronounced than this of t_{fc}.

All the investigated geometric (t_p; t_{fc}; g; Z_1 Z_2; d; D; and t_{rs}) and material (Young's modulus (E); the 0.2% proof stress ($\sigma_{0.2}$); and the ultimate stress (σ_u)) parameters were considered while formulating each of the developed expressions for K_i; K_p; M_o; and N (Table 4), and those, that were found to have an insignificant effect on the accuracy of an equation, were ignored for simplification (e.g. t_{fc} in the case of M_o). Moreover, some parameters were not taken into consideration although they had relatively non-low exponents, because (given their limited range) including or not including them in specific expressions did not have a noticeable impact on the accuracy of results. For instance, the inclusion of E which has a very limited range (from 195,000 to 220000 N/mm^2 [43]) did not enhance the effectiveness of the equations of K_p; M_o; and N, and thus E has not been included in these equations despite having moderately high exponents.

Using the developed analytical equations provided in Table 4, the four connection parameters for the 180 stainless steel extended end-plate connections, numerically investigated in Sections 3 and 4, were computed and then verified. As shown in Table 5, the analytical results exhibited good agreement with finite element data whether for stiffened or unstiffened connections.

Fig. 15 compares the FE and analytical key parameters for the 180 joints researched in the parametric study. From the comparison, it is evident that the accuracy of the derived formulas is higher in the case of K_i than in the case of K_p (Fig. 15(a)). This can be attributed to the uncertainties associated with the inelastic response of connections, due to material nonlinearity; complex interactions; and the formation of plastic hinges, which make the prediction of inelastic behavior relatively complicated when compared to the elastic response. As for M_o and N, the majority of their FE/analytical ratios lie between 1.1 and 0.9, which indicates a very good correlation between their numerical and analytical values (Fig. 15(b)).

5.3. Prediction of entire moment-rotation responses

Depending on Richard and Abbott expression [67] given by Eq. (2)

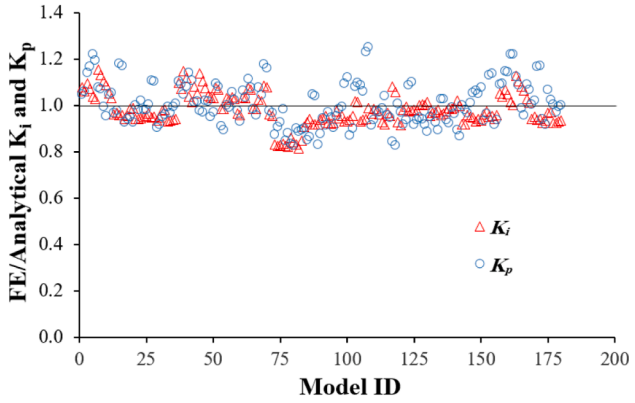

(a) Elastic and plastic stiffness

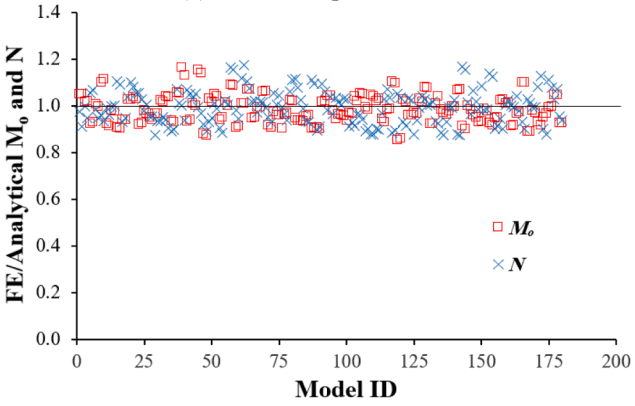

(b) Reference moment and curve shape factor

Fig. 15. Comparison of FE and analytical connection key parameters for the 180 cases studied in the parametric investigation.

Table 5
Performance of the analytical model in predicting the four parameters K_i, K_p, M_o and N.

End-plate stiffeners	Statistical parameters	$\frac{K_{i,FE}}{K_{i,Analytical}}$	$\frac{K_{p,FE}}{K_{p,Analytical}}$	$\frac{M_{o,FE}}{M_{o,Analytical}}$	$\frac{N_{FE}}{N_{Analytical}}$	No. of verifications
Unstiffened	Average	0.999	1.018	0.992	0.993	66
	COV (%)	9.8	9.9	7.5	6.1	
Stiffened	Average	0.970	0.995	0.984	0.993	114
	COV (%)	4.1	8.1	5.2	7.8	

and on the key connections parameters analytically calculated (in the previous subsection) for the 180 connections considered in the parametric study, the entire analytical moment-rotation curves for these joints were generated and subsequently compared with the numerically-predicted curves. Fig. 16 and Table 6 show comparisons of finite-element and analytical results for ten different joints carefully chosen to provide a proper representation of the 180 studied cases; the ten joints include ones whose analytical predictions for the four key parameters (computed using Eqs. (3) to (10)) have considerable disagreement with the numerical results, and also comprise models with highly-accurate predictions. It is should be noted that, as there is no formula limiting the progress of the analytical curves, they were plotted until maximum rotations calculated numerically, as illustrated in Fig. 16. This deficiency in the suggested analytical model will be discussed in detail (and dealt with) in Section 5.4.

From the table and the figure, it is clear that the analytically-predicted M-Φ responses are in excellent agreement with those generated by finite element analysis. For all cases including critical ones (i.e. those with relatively less-accurate key parameters estimations), there was no noticeable difference between the FE and analytical outcomes in the elastic range of response, while quite minor discrepancies have been noticed in a few cases at the post-elastic portion of the moment-rotation curves.

Referring again to Table 6 and Fig. 16, the proposed analytical model was capable of working out the moment at 30 mrad ($M_{j,30}$) with a high degree of accuracy. The average error in determining $M_{j,30}$ was less than, respectively, 5% for unstiffened connections and 4% for stiffened ones, with only about 3% of the models with deviations greater than 10%. In most cases, these errors, which were calculated at 30 mrad, decreased with increasing the rotation until reaching the ultimate moment, as depicted in Fig. 16. Detailed comparisons between numerical and analytical ultimate moment and rotation capacities are presented in the following subsections.

5.4. Development and validation of functions for the rotation corresponding to ultimate moment

As described in Section 5.3, the suggested analytical model (Eqs. (3) to (10)) showed considerable accuracy in reproducing the FE moment-rotation response of joints, however, it had an obvious deficiency; the analytically-generated curves can advance endlessly with no particular ultimate moment/rotation (this was the reason for plotting them, in Fig. 16, up to numerically-calculated maximum rotations). To overcome this deficiency (i.e. to make the proposed analytical technique able to independently predict the complete M-Φ response of connections, based only on the connections' properties without any inputs from finite element simulations), expressions for the ultimate moment or the rotation corresponding to it should be formulated.

Employing nonlinear regression analysis of numerical data and utilizing the same form of equation previously used for the four parameters' functions (Section 5.2), equations for the ultimate rotation of stainless steel extended end-plate joints were derived in terms of the geometrical and material characteristics investigated in the parametric study (Sections 3 and 4). The derived ultimate rotation equations for unstiffened and stiffened connections are given in Table 7.

Depending on the suggested functions, the rotation capacities of the stainless steel beam-to-column joints researched in the parametric investigation were determined, and then validated against FE data. Table 8 presents an evaluation of the performance of the ultimate rotation functions by means of statistical parameters. The table shows a significant correlation between the analytical and numerical results whether for unstiffened or stiffened joints, indicating that the derived expressions can help in overcoming the aforementioned deficiency of Eqs. (3) to (10).

5.5. Prediction of ultimate moment capacity

Using Richard-Abbott formula (Eq. (2)); the key connection parameters' functions (Eqs. (3) to (10)); in addition to the functions suggested for the maximum rotation (Eqs. (11) to (12)), the ultimate moment capacities for the 180 joints examined in the FE parametric study were calculated and compared with the corresponding numerical results.

Fig. 17 depicts a comparison of the FE and analytical maximum moments for the considered 180 cases. As shown in the figure, an excellent agreement can be observed between the numerically- and the analytically-estimated ultimate moments ($M_{j,\max}$). The average error (for all the analyzed joints) in predicting $M_{j,\max}$ was approximately 3.75%, while the maximum error was below 10%. These minor discrepancies demonstrate the great accuracy of the developed equations.

The entire analytical and FE moment-rotation responses for the joints were compared once again (they were compared earlier in Section 5.3), but this time the analytical curves were drawn until analytically-calculated maximum rotations, as illustrated in Fig. 18. From the figure, it can be seen that a close correspondence was obtained between the analytical and numerical ultimate capacities and overall M-Φ responses.

5.6. Further verification

In this subsection, the suggested analytical method is further evaluated by FE results for connection configurations other than those studied in the parametric analysis and employed for the calibration of the developed equations. A total of 36 cases, with geometric properties different from those parametrically-investigated in Sections 3 and 4, were considered, in order to check the effectiveness of the proposed method over a wide range of parameters' values.

The columns and beams in all joints examined in the further verification had an outer depth of 300 mm; a flange width of 200 mm; and a web thickness of 8 mm. As for flange thickness, it was 12 mm for the beams and varied in the case of columns, as described in Table 9 which lists the values of the parameters investigated in this supplementary assessment. The details of all the cases studied in the further verification can be found in Eladly's dataset [59].

Table 10 and Fig. 19 compare the analytical and FE key results (i.e. initial stiffness; moment at 30 mrad; ultimate moment; rotation corresponding to ultimate moment; and general moment-rotation behavior) for joints researched in the further verification, whilst Fig. 20 shows an evaluation of the suggested model's ability to calculate the moment capacity for the additional connection configurations. From the table and the figures, the suggested simplified technique continued to deliver accurate predictions for the overall M-Φ response of stainless steel extended end-plate joints. The average error in determining the maximum moment for the 36 additional cases was around 6%, whereas the ultimate error did not exceed 10%. Taking into consideration the complicated interactions and the nonlinear material response inherent in the studied connection type, it can be said that the accuracy achieved by the proposed simple method is satisfactory enough for structural applications.

5.7. Applications and limitations of the suggested analytical method

Although the analytical method developed in the preceding subsections demonstrated a high predictive performance, however, it has its limitations:

- The derived equations were only validated against the results of non-preloaded connections, due to the unavailability of data for stainless steel beam-to-column joints with preloaded bolts at the time of the study. Thus, the suggested method is not directly applicable to the latter type of connections until their test results become available and are utilized to recalibrate the equations. This is in accordance

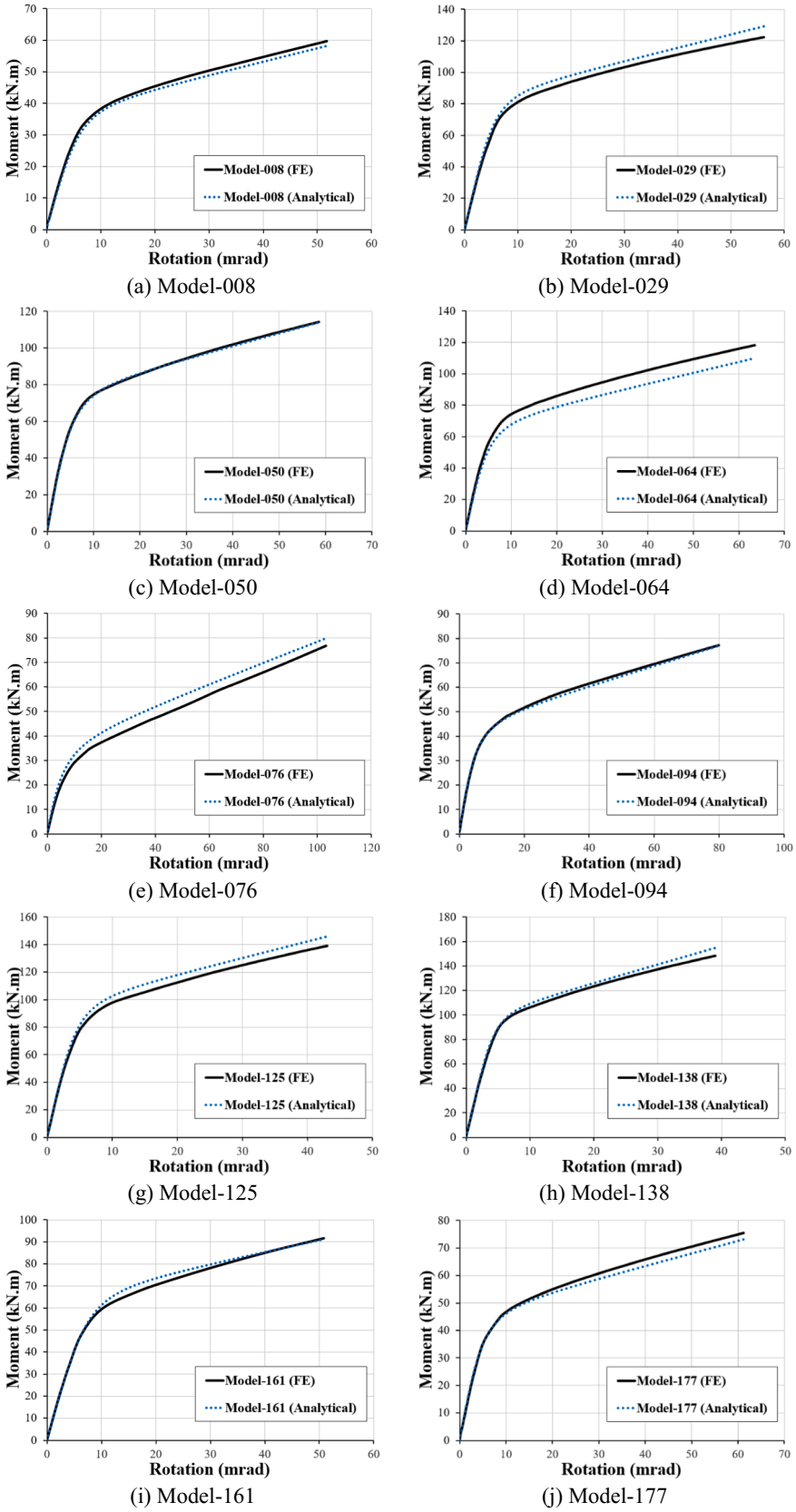

Fig. 16. Comparison of FE and analytical moment-rotation curves (plotted until maximum rotations calculated from FE results).

Table 6
Comparison of FE and analytical results (the geometric and material properties of the models are described in Eladly's dataset [59]).

Model ID	$\frac{K_{i,Analytical}}{K_{i,FE}}$	$\frac{K_{p,Analytical}}{K_{p,FE}}$	$\frac{M_{o,Analytical}}{M_{o,FE}}$	$\frac{N_{Analytical}}{N_{FE}}$	$M_{j,30,FE}(kN.m)$	$M_{j,30,Analytical}(kN.m)$	Discrepancies in $M_{j,30}$(%)
Model-008	0.88	0.93	1.00	1.06	50.08	48.85	−2.46
Model-029	1.07	1.11	1.03	1.14	103.09	106.95	3.74
Model-050	0.98	1.03	0.98	1.05	94.36	93.94	−0.44
Model-064	0.94	0.93	0.93	0.93	94.61	86.53	−8.54
Model-076	1.20	1.01	1.11	1.00	42.42	46.86	10.47
Model-094	1.04	1.06	0.96	0.96	57.15	55.84	−2.31
Model-125	1.05	1.09	1.03	1.14	124.88	130.19	4.25
Model-138	1.01	1.08	1.02	1.00	137.42	141.25	2.79
Model-161	0.99	0.82	1.10	1.00	78.06	79.60	1.97
Model-177	1.04	0.99	0.95	0.97	60.75	58.67	−3.42

Table 7
Ultimate rotation expressions developed for unstiffened and stiffened stainless steel extended end-plate joints.

	Parameter	Unit	Function	
Unstiffened	$\Phi_{j,u}$	*rad*	$0.60849 \times t_p^{1.0049} \times t_{fc}^{0.2978} \times g^{0.253} \times (d\text{-}Z_2)^{0.559} \times (Z_1\text{-}d)^{0.1255} \times d^{-1.033} \times D^{1.21} \times \sigma_{0.2}^{-0.0995}$	(11)
Stiffened	$\Phi_{j,u}$	*rad*	$1.820635 \times t_p^{1.03} \times t_{fc}^{0.317} \times g^{0.19} \times (d\text{-}Z_2)^{0.585} \times (Z_1\text{-}d)^{0.091} \times d^{-1.122} \times D^{1.42} \times \sigma_{0.2}^{-0.1704} \times t_{rs}^{0.252}$	(12)

[Note]: The geometric and material characteristics are expressed in mm and N/mm^2, respectively.

Table 8
Performance of the suggested equations in predicting ultimate rotation ($\Phi_{j,u}$).

End-plate stiffeners	Statistical parameters	$\frac{\Phi_{j,u,FE}}{\Phi_{j,u,Analytical}}$	No. of verifications
Unstiffened	Average	1.003	66
	COV (%)	9.1	
Stiffened	Average	1.032	114
	COV (%)	8.6	

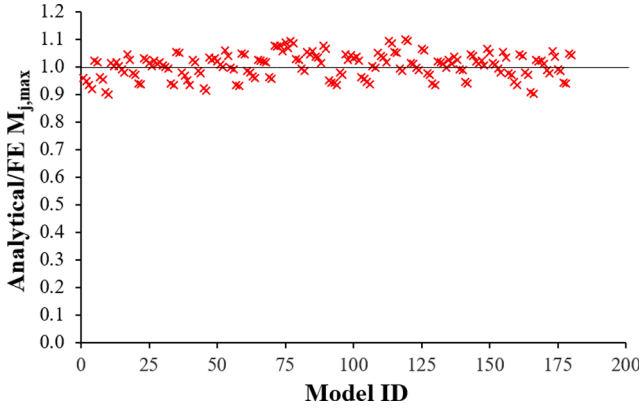

Fig. 17. Comparison of FE and analytical ultimate moment capacities for the 180 joints investigated in the parametric study.

with the recommendations of Eurocode 3 - Part 1.4 [43] which restricts the use of preloaded bolts in stainless steel bolted connections, stipulating that their acceptability in a certain application must be proved by experimental evidence.

- In all joints examined in the study, A80 bolts (the only austenitic stainless steel bolts classified as high-strength [68]) were employed for connection. Hence, the suggested method, in its present state, may not be usable for joints with bolts of other property classes (e.g. A50 –soft– or A70 –cold worked– bolts [68]).
- In terms of failure modes, the proposed analytical method was calibrated and verified against connections whose failure took place due to bolts fracture in tension. This agrees with previous studies on stainless steel extended end-plate joints [38,41,42], in all of which the failure of connections was prompted by tension bolts' failure. The reason that this type of failure is the dominant in this type of connections was discussed in Section 4. It is noteworthy that this failure mode is preferred over other failure patterns, since failure due to fracture in connecting elements is less detrimental and easier to repair than damage to connected members (columns and beams). Hence, most international design standards formulate their design rules so that the failure becomes confined to the connecting elements; that fact greatly diminishes the impact of the above limitation. Nonetheless, it must be said that the suggested analytical formulae can be reverified once new grades of high-strength stainless steel bolts with higher plastic strain at fracture are introduced.
- With regard to the applied loading type, the developed equations have been able to predict the *M-Φ* curves for connections subjected to monotonic bending moment, but their ability in the case of cyclically-loaded joints was not considered.
- The last limitation of the suggested analytical technique is related to the material properties of connected members and end-plate. As the study has focused exclusively on austenitic stainless steel grades, the technique's applicability to other grades of stainless steel (e.g. lean duplex) is conditional upon proper verification.

Three of the above five limitations are associated with using the austenitic type of stainless steel. Given the fact that this type is the most commonly utilized stainless steel type in the construction industry, the two relevant limitations are not that restrictive.

Taking the advantages and limitations of the proposed method into consideration, it can be stated that this method offers a simple but accurate analytical solution for predicting the entire moment-rotation characteristics of monotonically-loaded austenitic stainless steel extended end-plate connections with non-preloaded high-strength bolts. Once more experimental investigations become available, the suggested technique can be effortlessly revalidated (and recalibrated if required). To ease its use, an online worksheet, automating the calculations incorporated into it, has been attached to Eladly's dataset [59].

The suggested analytical method can help other researchers and structural design engineers to check their results, perform quick parametric studies, or carry out a swift assessment of the stiffness/strength of extended end-plate connections before conducting a detailed (and in many cases expensive) numerical analysis. More importantly, the FE and analytical study reported in this paper can pave the way for similar studies on other connection types widely-used in construction. Carrying out such studies will provide both (i) understanding of the response of different types of stainless steel connections, and (ii) powerful analytical tools that can accurately predict the moment-rotation response of connections. Having this understanding in addition to accurate analytical models (that can be readily used for generating data for thousands of cases) may facilitate a detailed assessment of design provisions of

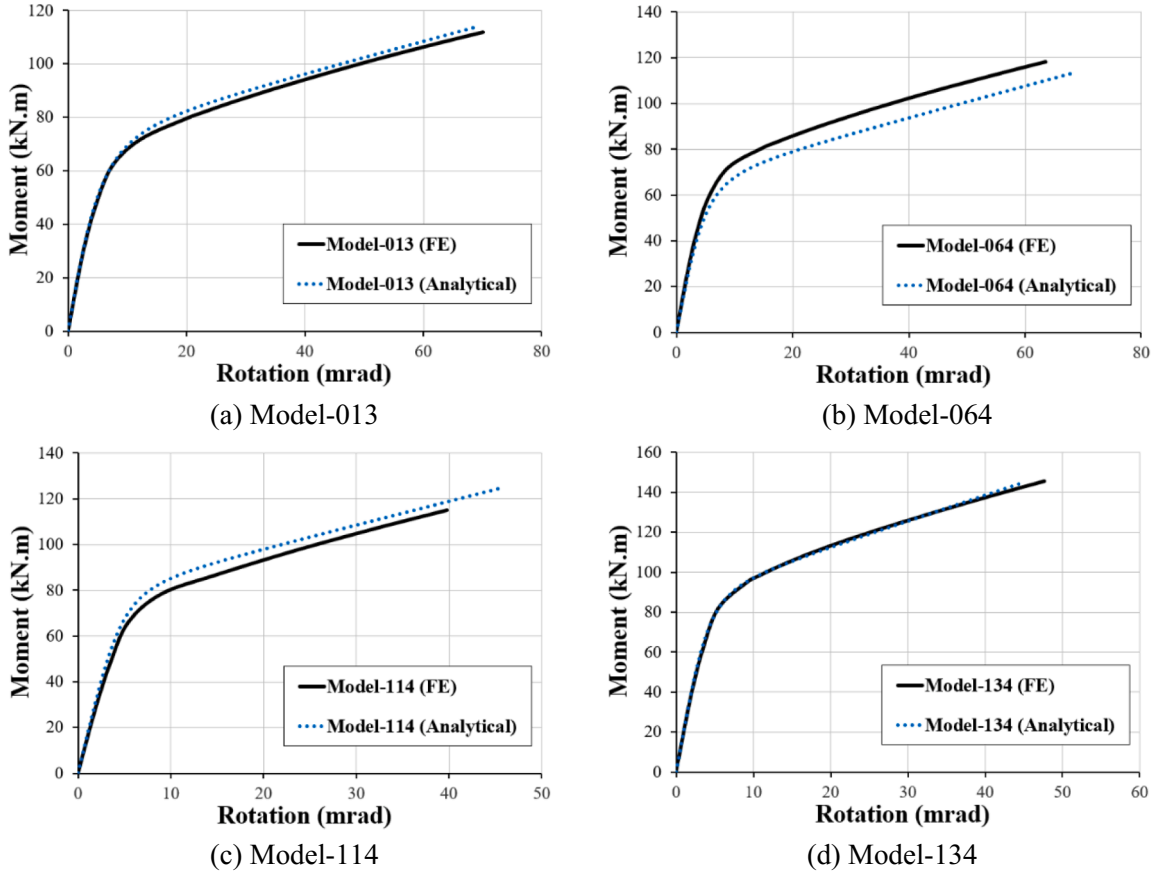

Fig. 18. Comparison of FE and analytical moment-rotation responses (the analytical curves are plotted until maximum rotations calculated analytically).

Table 9
Values of geometric and material parameters considered in the further verification (see Fig. 1(b) for the meanings of symbols).

t_p (mm)	t_{fc} (mm)	g (mm)	Z_1 (mm)	Z_2 (mm)	d (mm)	D (mm)	End-plate rib stiffeners	Stainless steel grade
12/14/16/18/20	12/16/20	108	344	232	300	16/20/24	Unstiffened/Stiffened t_{rs} = 6 mm/Stiffened t_{rs} = 10 mm	EN 1.4301

Table 10
Comparison of FE and analytical results for additional models investigated in the further verification (the geometric properties of each model are detailed in Eladly's dataset [59]).

Model ID	$\frac{K_{i,Analytical}}{K_{i,FE}}$	$\frac{M_{j,30,Analytical}}{M_{j,30,FE}}$	$\frac{M_{j,max,Analytical}}{M_{j,max,FE}}$	$\frac{\Phi_{j,u,Analytical}}{\Phi_{j,u,FE}}$
Model-182	1.02	0.95	0.91	0.98
Model-191	0.99	0.94	0.96	1.07
Model-194	0.90	0.98	0.96	1.00
Model-203	0.88	0.94	0.95	1.05

stainless steel connections in international standards. Following this thoroughgoing assessment, revisions to the design rules are expected, since these rules, in most current design standards, just mirror those developed for carbon steel joints neglecting the ductile nature of stainless steel.

6. Conclusions

Although deep understanding of connection behavior is vital for safe and economic design, limited research has been performed on beam-to-column bolted joints produced from stainless steel alloys. To fill this gap in knowledge, investigations should be undertaken in the area of structural stainless steel, considering the different connection typologies widely-used in construction (foremost among them extended end-plate joints). Based on a validated shell finite element modeling protocol, an exhaustive parametric study has been carried out on austenitic stainless steel extended end-plate beam-to-column connections. The study included 180 different connection configurations to examine the influence of geometric and material characteristics on the response of this connection type. The results of the investigation show that stainless steel extended end-plate joints have excellent ductility, with ductility indices ranging from 3.04 to 6.90 for the examined cases and with ultimate rotations fulfilling the rotation capacity recommended for beam-to-column joints in buildings located in earthquake-prone regions. Comparing the response of connections having end-plate stiffeners with that of unstiffened connections demonstrated how influential these stiffening elements are in the joints' behavior. The presence of end-plate stiffeners reduced the stresses on connected members, leading to enhancements in ultimate moment and dissipative energy of around 24% and 19%, respectively. This enhanced performance of stiffened stainless steel extended end-plate joints can accommodate the demands, for considerable moment and energy dissipation capacities, experienced in certain extreme events (e.g. earthquakes).

Exploiting the numerically-generated results for the 180 connections studied in the comprehensive parametric analysis, a simplified analytical method for predicting the M-Φ response of stainless steel extended end-plate connections was proposed. A series of analytical equations

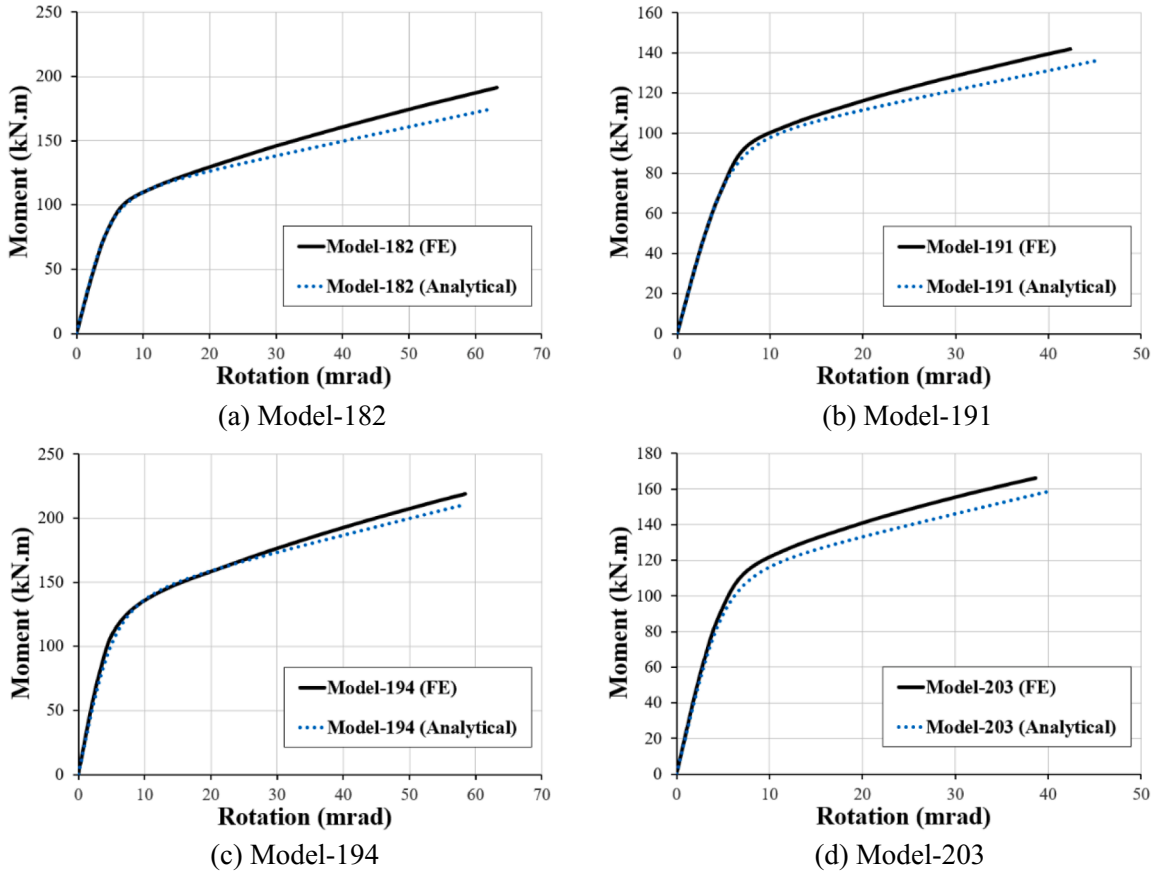

Fig. 19. Comparison of FE and analytical moment-rotation curves for joints examined in the further verification.

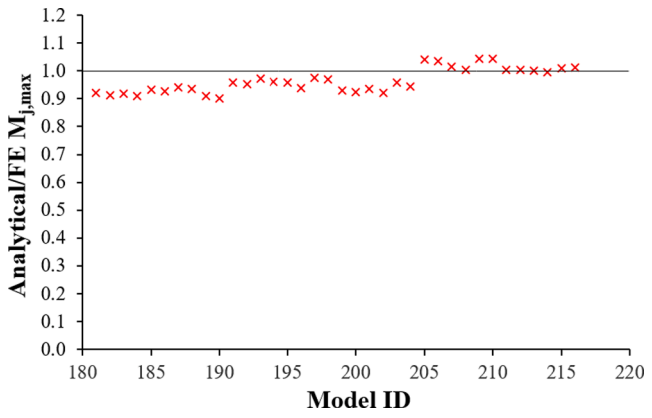

Fig. 20. Performance of the analytical method in predicting the ultimate moment of connections considered in the further verification (Models 181–216).

was derived in terms of basic connection geometric and material properties, taking into account the significant strain hardening of austenitic stainless steel. By validating the analytical results against the finite element models, it is evident that the analytical model is capable of providing accurate estimations whether for the key connection parameters (e.g. initial stiffness; strain- hardening stiffness; and maximum moment and rotation) or for the complete moment-rotation behavior. For the 180 cases, the average deviation between the numerically- and analytically-calculated ultimate moment capacity was 4%. Furthermore, an additional verification of the proposed method was conducted using numerical results for connection configurations other than those investigated in the parametric study. The further verification confirmed the accuracy of the developed equations in computing the key results and reproducing the entire *M-Φ* curves of connections. The worst error in determining the moment capacity for the 216 joints examined (including 180 joints in the parametric analysis in addition to 36 joints in the further verification) was below 10%. This satisfactory accuracy along with the simplicity of the suggested method can strongly promote its utilization in future research as well as in practical structural applications. To facilitate this prospective utilization, an online worksheet was built based on the proposed equations and has been linked to the full dataset [59].

The data of the 180 connections investigated in the parametric study together with the developed analytical model can be employed in future studies aiming to perform a thorough assessment of the current design provisions of stainless steel joints, which mirror those of carbon steel connections without completely considering the distinguishing nonlinear material behavior and strain hardening properties of stainless steel.

Declaration of Competing Interest

The authors declare that they have no known competing financial interests or personal relationships that could have appeared to influence the work reported in this paper.

References

[1] Rossi B. Discussion on the use of stainless steel in constructions in view of sustainability. Thin-Walled Struct. 2014;83:182–9.
[2] Gedge G. Structural uses of stainless steel —buildings and civil engineering. J. Constr. Steel Res. 2008;64(11):1194–8.
[3] Baddoo NR. Stainless steel in construction: a review of research, applications, challenges and opportunities. J. Constr. Steel Res. 2008;64(11):1199–206.

[4] Gardner L. The use of stainless steel in structures. Prog. Struct. Eng. Mater. 2005;7(2):45–55.
[5] Cashell KA, Baddoo NR. Ferritic stainless steels in structural applications. ThinWalled Struct. 2014;83:169–81.
[6] Di Sarno L, Elnashai AS, Nethercot DA. Seismic performance assessment of stainless steel frames. J. Constr. Steel Res. 2003;59(10):1289–319.
[7] Di Sarno L, Elnashai AS, Nethercot DA. Seismic retrofitting of framed structures with stainless steel. J. Constr. Steel Res. 2006;62(1–2):93–104.
[8] Zhou F, Li L. Experimental study on hysteretic behavior of structural stainless steels under cyclic loading. J. Constr. Steel Res. 2016;122:94–109.
[9] Banisheikholeslami A, Behnamfar F, Ghandil M. A beam-to-column connection with visco-elastic and hysteretic dampers for seismic damage control. J. Constr. Steel Res. 2016;117:185–95.
[10] Sakurai S, Ellingwood BR, Kushiyama S. Probabilistic study of the behavior of steel frames with partially restrained connections. Eng. Struct. 2001;23(11):1410–7.
[11] Mohammadi M, Emami SMM. Multi-bay and pinned connection steel infilled frames; an experimental and numerical study. Eng. Struct. 2019;188:43–59.
[12] Eladly MM. Numerical study on masonry-infilled steel frames under vertical and cyclic horizontal loads. J. Constr. Steel Res. 2017;138:308–23.
[13] Sakr MA, Eladly MM, Khalifa T, El-Khoriby S. Cyclic behaviour of infilled steel frames with different beam-to-column connection types. Steel Compos. Struct. 2019;30(5):443–56.
[14] Errera SJ, Popowich DW, Winter G. Bolted and welded stainless steel connections. J. Struct. Eng. ASCE 1974;100(6):1279–96.
[15] Kim TS, Kuwamura H. Finite element modeling of bolted connections in thin-walled stainless steel plates under static shear. Thin-Walled Struct. 2007;45(4):407–21.
[16] Kim TS, Kuwamura H, Cho TJ. A parametric study on ultimate strength of single shear connections with curling. Thin-Walled Struct. 2008;46(1):38–53.
[17] Bouchaïr A, Averseng J, Abidelah A. Analysis of the behaviour of stainless steel bolted connections. J. Constr. Steel Res. 2008;64(11):1264–74.
[18] Salih EH, Gardner L, Nethercot DA. Bearing failure in stainless steel bolted connections. Eng. Struct. 2011;33(2):549–62.
[19] Salih EH, Gardner L, Nethercot DA. Numerical study of stainless steel gusset plate connections. Eng. Struct. 2013;49:448–64.
[20] Cai Y, Young B. Structural behavior of cold-formed stainless steel bolted connections. Thin-Walled Struct. 2014;83:147–56.
[21] Cai Y, Young B. Bearing resistance design of stainless steel bolted connections at ambient and elevated temperatures. Steel Compos. Struct. 2018;29(2):273–86.
[22] Cai Y, Young B. Behavior of cold-formed stainless steel single shear bolted connections at elevated temperatures. Thin-Walled Struct. 2014;75:63–75.
[23] Cai Y, Young B. Transient state tests of cold-formed stainless steel single shear bolted connections. Eng. Struct. 2014;81:1–9.
[24] Cai Y, Young B. Fire resistance of stainless steel single shear bolted connections. Thin-Walled Struct. 2018;130:332–46.
[25] Cai Y, Young B. Structural behaviour of cold-formed stainless steel bolted connections at post-fire condition. J. Constr. Steel Res. 2019;152:312–21.
[26] Cai Y, Young B. Carbon steel and stainless steel bolted connections undergoing unloading and re-loading processes. J. Constr. Steel Res. 2019;157:337–46.
[27] Stranghöner N, Afzali N, Vries P, Schedin E, Pilhagen J, Cardwell S. Slip-resistant bolted connections of stainless steel. Steel Constr. 2017;10(4):333–43.
[28] Stranghöner N, Afzali N, Vries P, Schedin E, Pilhagen J. Slip factors for slip-resistant connections made of stainless steel. J. Constr. Steel Res. 2019;152:235–45.
[29] Afzali N, Stranghöner N, Pilhagen J, Manninen T, Schedin E. Viscoplastic deformation behaviour of preloaded stainless steel connections. J. Constr. Steel Res. 2019;152:225–34.
[30] Yang L, Cui Y, Wei X, Li M, Zhang Y. Strength of duplex stainless steel fillet welded connections. J. Constr. Steel Res. 2019;152:246–60.
[31] Yuan HX, Hu S, Du XX, Yang L, Cheng XY, Theofanous M. Experimental behaviour of stainless steel bolted T-stub connections under monotonic loading. J. Constr. Steel Res. 2019;152:213–24.
[32] Feng R, Young B. Design of cold-formed stainless steel tubular joints at elevated temperatures. Eng. Struct. 2012;35:188–202.
[33] Feng R, Young B. Theoretical analysis of cold-formed stainless steel tubular joints. Eng. Struct. 2015;83:99–115.
[34] Feng R, Lin J, Mou X. Experiments on hybrid tubular K-joints with circular braces and square chord in stainless steel. Eng. Struct. 2019;190:52–65.
[35] Feng R, Liu Y, Zhu J. Tests of CHS-to-SHS tubular connections in stainless steel. Eng. Struct. 2019;199.
[36] Hasan MJ, Ashraf M, Uy B. Moment-rotation behaviour of top-seat angle bolted connections produced from austenitic stainless steel. J. Constr. Steel Res. 2017;136:149–61.
[37] Elflah M, Theofanous M, Dirar S, Yuan H. Behaviour of stainless steel beam-to-column joints – Part 1: Experimental investigation. J. Constr. Steel Res. 2019;152:183–93.
[38] Elflah M, Theofanous M, Dirar S. Behaviour of stainless steel beam-to-column joints – Part 2: Numerical modelling and parametric study. J. Constr. Steel Res. 2019;152:194–212.
[39] Elflah M, Theofanous M, Dirar S, Yuan H. Structural behaviour of stainless steel beam-to-tubular column joints. Eng. Struct. 2019;184:158–75.
[40] Hasan MJ, Al-Deen S, Ashraf M. Behaviour of top-seat double web angle connection produced from austenitic stainless steel. J. Constr. Steel Res. 2019;155:460–79.
[41] Bu Y, Wang Y, Zhao Y. Study of stainless steel bolted extended end-plate joints under seismic loading. Thin-Walled Struct. 2019;144.
[42] Gao JD, Yuan HX, Du XX, Hu XB, Theofanous M. Structural behaviour of stainless steel double extended end-plate beam-to-column joints under monotonic loading. Thin-Walled Struct. 2020;151.
[43] EN 1993-1-4+A1, Eurocode 3: Design of Steel Structures - Part 1.4: General Rules Supplementary Rules for Stainless Steel, CEN, 2015.
[44] EN 1993-1-8, Eurocode 3: Design of Steel Structures - Part 1.8: Design of Joints, British Standards Institution, CEN, 2005.
[45] Wang M, Shi Y, Wang Y, Shi G. Numerical study on seismic behaviors of steel frame end-plate connections. J. Constr. Steel Res. 2013;90:140–52.
[46] El-Khoriby S, Sakr MA, Khalifa TM, Eladly MM. Modelling and behaviour of beam-to-column connections under axial force and cyclic bending. J. Constr. Steel Res. 2017;129:171–84.
[47] Eladly MM. Behaviour of stainless steel beam-to-column bolted connections–Part 1: Simplified FE model. J. Constr. Steel Res. 2020;164.
[48] ABAQUS. Analysis User's Manual. Version 6.12, ABAQUS Inc. Dassault Systèmes, USA 2012.
[49] Rasmussen KJR. Full-range stress-strain curves for stainless steel alloys. J. Constr. Steel Res. 2003;59(1):47–61.
[50] Ghobarah A, Osman A, Korol RM. Behaviour of extended end-plate connections under cyclic loading. Eng. Struct. 1990;12(1):15–27.
[51] Bernuzzi C, Zandonini R, Zanon P. Experimental analysis and modelling of semi-rigid steel joints under cyclic reversal loading. J. Constr. Steel Res. 1996;38(2):95–123.
[52] Shi G, Shi Y, Wang Y. Behaviour of end-plate moment connections under earthquake loading. Eng. Struct. 2007;29(5):703–16.
[53] Tartaglia R, D'Aniello M, Rassati GA, Swanson JA, Landolfo R. Full strength extended stiffened end-plate joints: AISC vs recent European design criteria. Eng. Struct. 2018;159:155–71.
[54] Tartaglia R, D'Aniello M, Zimbru M, Landolfo R. Finite element simulations on the ultimate response of extended stiffened end-plate joints. Steel Compos. Struct. 2018;27(6):727–45.
[55] ElSabbagh A, Sharaf T, Nagy S, ElGhandour M. Behavior of extended end-plate bolted connections subjected to monotonic and cyclic loads. Eng. Struct. 2019;190:142–59.
[56] Foley CM, Vinnakota S. Toward design office moment-rotation curves for end-plate beam-to-column connections. J. Constr. Steel Res. 1995;35(2):217–53.
[57] Dessouki AK, Youssef AH, Ibrahim MM. Behavior of I-beam bolted extended end-plate moment connections. Ain Shams Eng. J. 2013;4(4):685–99.
[58] Real E, Arrayago I, Mirambell E, Westeel R. Comparative study of analytical expressions for the modelling of stainless steel behaviour. Thin-Walled Struct. 2014;83:2–11.
[59] Eladly MM. Data for numerical and analytical study of stainless steel beam-to-column extended end-plate connections. Mendeley Data 1 2020. https://doi.org/10.17632/3b8rywn9db.1.
[60] Wilkinson S, Hurdman G, Crowther AA. Moment resisting connection for earthquake resistant structures. J. Constr. Steel Res. 2006;62:295–302.
[61] A.M. Girão Coelho, F.S.K. Bijlaard, L. Simões da Silva, Experimental assessment of the ductility of extended end plate connections, Eng. Struct. 26 (2004) 1185-1206.
[62] Girão Coelho AM, Bijlaard FSK. Experimental behaviour of high strength steel end plate connections. J. Constr. Steel Res. 2007;63:1228–40.
[63] P. Zanon, R. Zandonini, Experimental analysis of end plate connections, Proceedings of the State of the Art Workshop on Connections and the Behaviour of Strength and Design of Steel Structures, Cachan 1988, pp. 41-51.
[64] Girão Coelho AM, da Silva LS, Bijlaard FSK. Ductility analysis of bolted extended end plate beam-to-column connections in the framework of the component method. Steel Compos. Struct. 2006;6(1):33–53.
[65] Naeim F. The seismic design handbook. 2nd ed. Kluwer Academic Publishers; 2001. p. 418.
[66] Zoetemeijer P. A design method for the tension side of statically loaded, bolted beam-to-column connections. HERON 1974;20(1).
[67] Richard RM, Abbott BJ. Versatile elastic-plastic stress-strain formula. J. Eng. Mech. Div. 1975;101(4):511–5.
[68] EN ISO 3506-1, Mechanical properties of corrosion-resistant stainless steel fasteners – Part 1: Bolts, screws and studs (ISO 3506-1:2009), 2009.
[69] Eladly MM. Analytical study of unstiffened extended end-plate connections produced from austenitic stainless steel. Proceedings of the Cold-Formed Steel Research Consortium Colloquium 2020.